

Hydrothermal synthesis and characterization of carbon-doped TiO_2 nanoparticles

Zafar Ali, Javaid Ismail, Rafaqat Hussain, A. Shah, Arshad Mahmood, Arbab Mohammad Toufiq, Shams ur Rahman

Citation: Chin. Phys. B . 2020, 29(11): 118102 . **doi:** 10.1088/1674-1056/ab9f29
Journal homepage: http://cpb.iphy.ac.cn; http://iopscience.iop.org/cpb

What follows is a list of articles you may be interested in

Uncovering the internal structure of five-fold twinned nanowires through 3D electron diffraction mapping

Xin Fu(付新)

Chin. Phys. B . 2020, 29(6): 068101 . **doi:** 10.1088/1674-1056/ab8370

Improved performance of back-gate MoS_2 transistors by NH_3-plasma treating high-*k* gate dielectrics

Jian-Ying Chen(陈建颖), Xin-Yuan Zhao(赵心愿), Lu Liu(刘璐), Jing-Ping Xu(徐静平)

Chin. Phys. B . 2019, 28(12): 128101 . **doi:** 10.1088/1674-1056/ab50fe

Germanene nanomeshes:Cooperative effects of degenerate perturbation and uniaxial strain on tuning bandgap

Yan Su(苏燕), Xinyu Fan(范新宇)

Chin. Phys. B . 2017, 26(10): 108101 . **doi:** 10.1088/1674-1056/26/10/108101

Geometrically induced *π*-band splitting in graphene superlattices

Yanpei Wei(魏艳佩), Tiantian Jia(贾甜甜), Gang Chen(陈刚)

Chin. Phys. B . 2017, 26(2): 028103 . **doi:** 10.1088/1674-1056/26/2/028103

Microstructure and photocatalytic activity of titanium dioxide nanoparticles

Li Chun-Yan, Wang Jiang-Bin, Wang Yi-Qian

Chin. Phys. B . 2012, 21(9): 098102 . **doi:** 10.1088/1674-1056/21/9/098102

Hydrothermal synthesis and characterization of carbon-doped TiO_2 nanoparticles*

Zafar Ali[1], Javaid Ismail[1], Rafaqat Hussain[2], A. Shah[3], Arshad Mahmood[3], Arbab Mohammad Toufiq[4], and Shams ur Rahman[1,†]

[1] *Department of Physics, COMSATS University Islamabad, Park Road, Islamabad* 45550, *Pakistan*
[2] *Department of Chemistry, COMSATS University Islamabad, Park Road, Islamabad* 45550, *Pakistan*
[3] *National Institute of Lasers and Optronics College, Pakistan Institute of Engineering and Applied Sciences (NILOP-C, PIEAS), Nilore* 45650, *Islamabad, Pakistan*
[4] *Department of Physics, Hazara University Mansehra, Mansehra* 21300, *Pakistan*

(Received 17 April 2020; revised manuscript received 3 June 2020; accepted manuscript online 23 June 2020)

We report the hydrothermal growth of pure and doped TiO_2 nanoparticles with different concentrations of carbon. The microstructure of the as-synthesized samples is characterized by x-ray diffraction (XRD), field emission scanning electron microscopy (FESEM), energy dispersive x-ray spectroscopy (EDX), and Raman spectroscopy to understand the structure and composition. The XRD patterns confirm the formation of anatase phase of TiO_2 with the average crystallite size is calculated to be in the range of 13 nm to 14.7 nm. The functional groups of these nanostructures are characterized by Fourier transformed infrared (FT-IR) spectroscopy, which further confirms the single anatase phase of the synthesized nanostructures. UV-visible absorption spectroscopy is used to understand the absorption behavior, which shows modification in the optical bandgap from 3.13 eV (pure TiO_2) to 3.74 eV (1.2 mol% C-doped TiO_2). Furthermore, the Ti^{3+} centers associated with oxygen vacancies are identified using electron paramagnetic resonance spectroscopy (EPR).

Keywords: titanium dioxide, hydrothermal synthesis, defect states, bandgap

PACS: 81.07.−b, 78.67.−n **DOI:** 10.1088/1674-1056/ab9f29

1. Introduction

Fabrication of nanostructured materials with controlled size and morphology is of importance to ensure their optimum performance in various device applications such as optics, mechanics, and electronics, because the size and shape of nanoparticles are key factors, which are under consideration while tailoring the properties of semiconductor materials.[1,2] Transition metal oxides (TMOs) have gained remarkable attention and recognition owing to their intriguing optical, electrical, and magnetic properties.[3–8] There has been a surge of research activity to exploit new functional materials in order to deal with the environmental pollution, global industrialization, and energy crisis with the ability to degrade pollutants and produce energy in an environmentally friendly manner.[9–11] Among these, titanium dioxide (TiO_2) is a binary transition metal oxide and widely studied material that has sparked the ongoing research due to its outstanding properties such as high refractive index, chemical stability, low cost, non-toxicity, resistant to photo-corrosion, and excellent optical transmittance.[12] TiO_2 naturally occurs in three crystalline polymorphs: anatase, rutile, and brookite. Both the anatase and brookite are metastable, whilst rutile is a stable phase.[13,14] At room temperature rutile has a bandgap of 3.06 eV,[15] 3.3 eV for brookite, and a wide bandgap of about 3.4 eV for anatase phase.[16]

Several attempts have been made to fabricate the doped TiO_2 nanostructures using various synthetic routes and to study the variation in their physical and chemical properties because in facilitating advanced technologies, the critical parameters such as the morphology and phase composition determine their suitability for multiple applications.[9] Bernard *et al.*[17] in their shape-dependent thermodynamic model reported that both the shape and phase stability of TiO_2 nanoparticles strongly depend on their surface chemistry. In particular, doping of TiO_2 with transition metals/non-metals has been widely investigated for a wide range of applications such as photocatalysis, water splitting, and N_2 reduction reaction, etc.[18–20] For instance, doping TiO_2 with metals/non-metals such as carbon,[21] nitrogen,[22] sulfur,[23] vanadium,[15] manganese,[16] iron,[17] nickel,[18] etc. has been reported to modify the bandgap of TiO_2 and extend its absorption to the visible region for photocatalysis.[24–27] Shao *et al.*[28] reported a reduction in the bandgap of rutile TiO_2 (3.0 eV to 2.67 eV) upon doping with carbon, which extended its working spectrum to the visible region. Noorimotlagh *et al.*[29] reported that the incorporation of carbon atoms decreases the size of TiO_2 nanoparticles as compared to pure samples and the absorption wavelength shifts to a higher wavelength region ($\lambda > 400$ nm). The present study deals with the synthesis of pure and carbon-doped TiO_2 with different

*The authors would like to thank the Higher Education Commission of Pakistan for providing funding (NRPU project 5349/Federal/NRPU/R&D/HEC/2016).
†Corresponding author. E-mail: shamsur_rehman@comsats.edu.pk
© 2020 Chinese Physical Society and IOP Publishing Ltd

concentrations using a facile hydrothermal method. The influences of varying amount of carbon concentration on the structural, morphological, and optical properties of TiO_2 nanostructures have been studied and discussed in detail.

2. Experimental details

2.1. Materials and methods

All chemicals and solvents are of analytical grade, and used without any further purification. Titanium (III) chloride ($TiCl_3$) solvent (ca.15%) and D(+)-glucose monohydrate ($C_6H_{12}O_6.H_2O$) are purchased from Honeywell (Burdick and Jackson). Ammonia (NH_3) solution ($\sim$ 35%) and HCl (37%) are purchased from Sigma Aldrich and Scharlau, respectively. Deionized water (DI) and ethanol are used during the synthesis.

TiO_2 nanoparticles (NPs) are synthesized by adopting the hydrothermal method. A 10 ml of $TiCl_3$ solution is mixed with HCl/DI water (3 : 17) solution in a flask. Then the solution is stirred and a small amount of glucose (0.0, 0.2 mol%, 0.6 mol%, and 1.2 mol%) is added during the stirring. For complete precipitation of TiO_2, ammonia solution (ca.25 ml) is added dropwise until the solution pH is tuned to 10. The solution is stirred at 60 °C for 30 min and then transferred into a teflon-lined stainless autoclave and heated in an oven at 180 °C for 24 hours. TiO_2 NPs are then separated from the solution by centrifugation and washed several times with absolute ethanol and DI water. The resultant product is dried in a vacuum oven at 80 °C for 24 hours. The samples obtained are labeled as P, C-1, C-2, and C-3, respectively.

3. Results and discussion

3.1. Structural analysis

Figure 1 depicts the x-ray diffraction (XRD) patterns of pure and different concentrations of glucose (0.0, 0.20 mol%, 0.60 mol%, and 1.20 mol%). The synthesized samples exhibit diffraction peaks at 25.21°, 37.80°, 47.94°, 54.02°, 54.99°, 62.70°, 68.82°, 69.94°, and 75.08° corresponding to the (101), (004), (200), (105), (211), (204), (116), (220), and (215) crystallographic planes, respectively. The peak positions are well-matched with standard anatase TiO_2 (JCPDS 00-021-1272)[30] and no extra carbon peaks were found in the crystal structure of TiO_2. The sharp peaks indicate the high crystallinity of all samples. No changes are observed in the crystal structure of the doped samples, which can be ascribed to the small concentration of carbon content. All the resulting samples are identified to have a homogenous anatase phase. The unit cell parameters for pure and 0.6% C-doped TiO_2 are calculated as $a = b = 3.7893$ Å, $c = 9.4921$ Å, and $a = b = 3.8224$ Å, $c = 9.4946$ Å, respectively, All the peaks are well indexed to the standard diffraction data as listed in JCPDS card No. 00-021-1272. The average crystallite sizes are calculated using the well known Scherrer equation. The calculated average crystallite size for pure and doped samples with varying carbon concentration is in the range of 13.3 nm to 14.74 nm. The elemental composition of the as-prepared pure and doped nanostructures is confirmed by energy dispersive x-ray (EDX) analysis as shown in Figs. 2(a) and 2(b). The EDX analysis reveals that carbon was successfully doped into the crystal structure of anatase TiO_2, without affecting the crystalline lattice planes of the TiO_2 crystal structure.

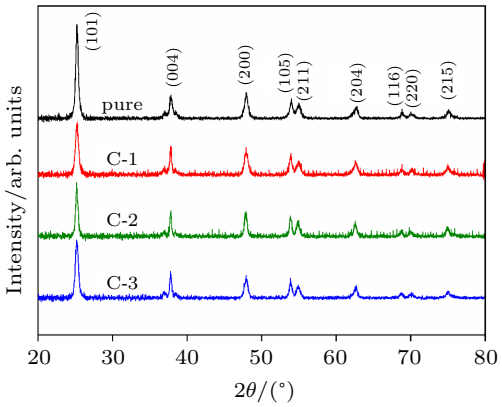


Fig. 1. The XRD patterns of pure and C-doped TiO_2 NPs synthesized by the hydrothermal approach.

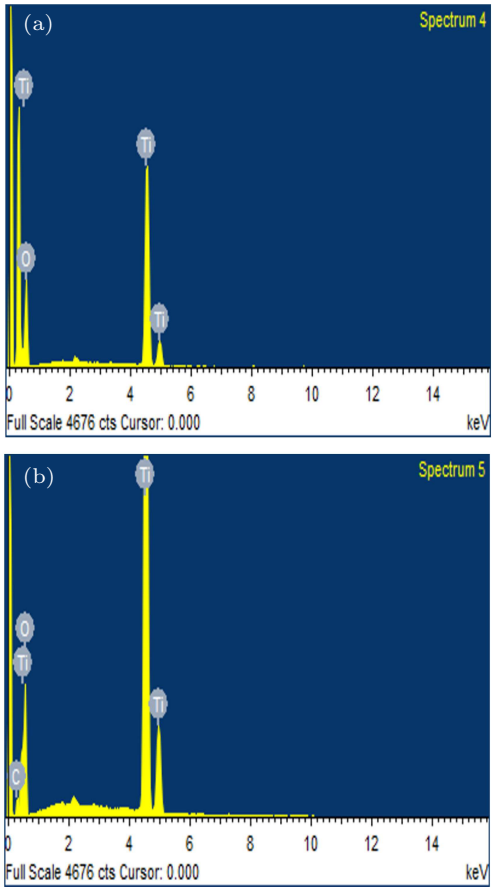


Fig. 2. The EDX spectrum of (a) pure and (b) 1.2% C-doped TiO_2 NPs.

3.2. Morphology and microstructure studies

SEM images of the pure and C-doped TiO_2 NPs were obtained with the help of field emission scanning electron microscope (Model, TESCAN MAIA3) housed with an Octane Elite EDAX detector. The measurements were performed at an accelerating voltage of 20 keV. Figure 3(a) shows the morphology of pure TiO_2 NPs. The TiO_2 NPs appear spherical and produce aggregates to form chunks of TiO_2. The morphology of NPs is observed to change with the inclusion of carbon up to 1.2 mol% as shown in Fig. 3(b). As is seen, the shape of NPs changes to elongated particles, indicating that carbon doping influences the morphology of TiO_2 NPs. Furthermore, it is evident from Fig. 3(b) that the morphology of the C-doped samples is more homogeneous and uniform as compared to the pure TiO_2 NPs.

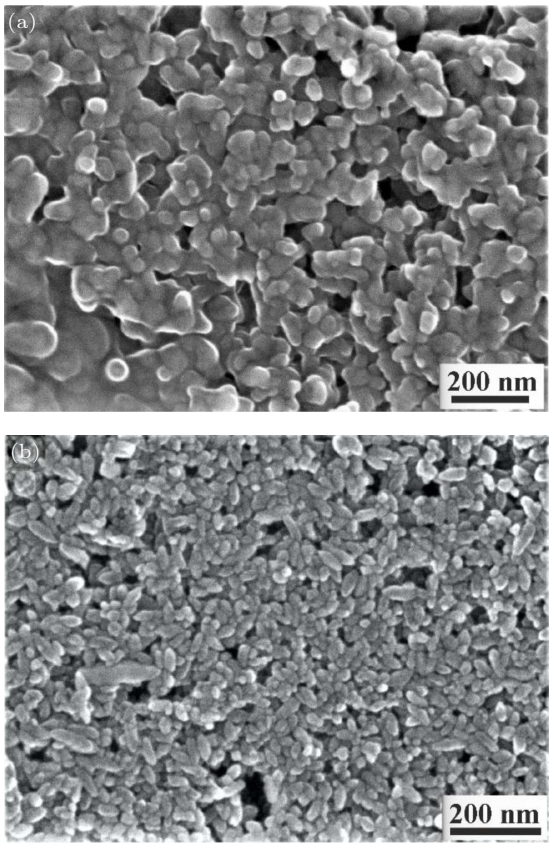


Fig. 3. The FESEM images showing the morphology of (a) pure TiO_2 and (b) 1.2% C-doped TiO_2 NPs.

3.3. Vibrational modes studies

Raman spectroscopy is used to investigate the vibrational modes of pure and carbon doped TiO_2 NPs. Figure 4 shows the Raman spectra of synthesized samples taken at room temperature. The instrument is equipped with an excitation source of 514 nm argon ion laser, and for focusing the incident beam, a 100× objective is used. A slight blueshift is observed due to carbon doping as compared to pure TiO_2. There are six active Raman vibration modes of anatase TiO_2 as E_g (139 cm^{-1}), E_g (196 cm^{-1}), B_{1g} (398 cm^{-1}), A_{1g} (516 cm^{-1}), B_{1g} (519 cm^{-1}), and E_g (448 cm^{-1}).[31] It is observed that E_g, B_{1g}, and A_{1g} vibration modes originated from symmetric stretching, symmetric bending, and antisymmetric bending vibrations of O–Ti–O in TiO_2 lattice, respectively.[32] These characteristic vibrational frequencies and their relative intensities confirm the anatase TiO_2 NPs and are consistent with the XRD analysis.

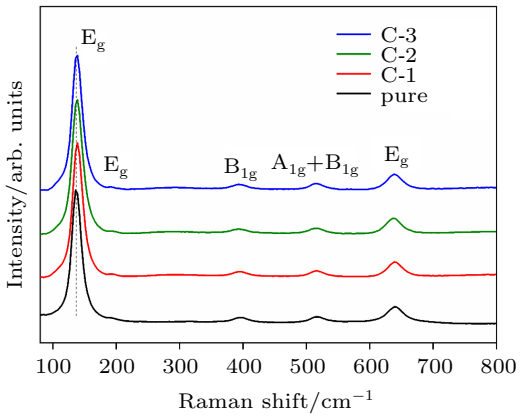


Fig. 4. Raman spectra of pure and C-doped TiO_2 NPs.

3.4. Functional group analysis

Fourier-transform infrared spectroscopy (FT-IR) is used to investigate the influence of carbon doping on the functional groups of TiO_2 NPs. Figure 5 depicts the FT-IR profile of pure and C-doped TiO_2 samples. The broadband which appears in all samples below 1000 cm^{-1} in the range 400–800 cm^{-1} is due to the stretching vibration of Ti–O–Ti and Ti–O–C functional groups[27,33] in the anatase phase. The spectra for the C-doped TiO_2 NPs shift towards higher wavenumbers as compared to the pure one and this could be ascribed to the carbon concentration in TiO_2 NPs. The band around 1429–1438 cm^{-1} is due to surface adsorbed CO_2. The broad peaks at 1633 cm^{-1} and 1635 cm^{-1} are due to the bending vibration of coordinated water.[27] The peaks are very broad at about 3200 cm^{-1}, implying that all the samples chemisorbed more water during the synthesis,[34] which shows the presence of hydroxyl group (OH) in the as-prepared NPs.

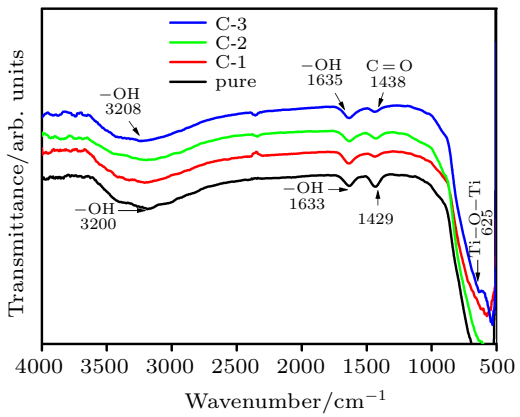


Fig. 5. The FT-IR spectra of pure and C-doped TiO_2 NPs.

3.5. Ultraviolet–visible absorption studies

Figure 6(a) shows the UV–visible absorption spectra of the pure and C-doped TiO_2 NPs. The spectra are recorded in the wavelength range of 200–800 nm at room temperature. The C-doped TiO_2 NPs show a significant blueshift as compared to pure TiO_2. The energy bandgap (E_g) is calculated using Tauc's equation[35]

$$(\alpha h\nu)^2 = A(h\nu - E_g), \tag{1}$$

where α is the optical absorption coefficient, h is the Plank's constant, ν is the frequency of the photon, A is an energy independent constant, and E_g is the optical bandgap energy of the NPs. The bandgap values of the prepared samples are determined by plotting $(\alpha h\nu)^2$ as a function of $E_g(h\nu)$ to intercept with the E_g axis as shown in Fig. 6(b). The bandgap values of the pure and 1.2% C-doped TiO_2 NPs are determined to be 3.13 eV and 3.74 eV, respectively. Carbon doping in TiO_2 has been previously reported to induce redshift in the absorption spectra.[36,37] However, in this work the bandgap values increase with the carbon content and show a blueshift compared to the pure sample (Table 1). It is known that the bandgap of oxide semiconductors is a function of particle size.[38] By reducing the particle size below a certain threshold, the electrons and holes in the nanocrystalline semiconductor are confined leading to quantum confinement effects.[38–40] As a result, the separation between the filled valence band and the empty conduction band is increased and a blueshift is observed in the absorption edge. The observations of blueshift in other TiO_2 systems have revealed that a systematic increase in the energy bandgap with increasing the doping content is due to the formation of new energy levels by the interaction of the dopant atoms with the host lattice.[41] For instance, Bhange *et al.*[41] found that a consistent increase in the bandgap of TiO_2 NPs with increasing Sn concentration is not due to the quantum size effect but due to the large crystallite size (larger than 10 nm). Linsebigler *et al.*[42] found that crystallite sizes larger than the Bohr radius cause the $1/R^2$ term approaching zero. In our work, the crystallite sizes are in the range of 13.3 nm to 14.74 nm. Therefore, for crystallite sizes larger than 10 nm the quantum confinement effect could be ruled out.[43]

Table 1. Bandgap of the undoped and doped TiO_2 NPs and their corresponding absorption wavelengths.

Doping concentration of glucose/mol%	Absorption wavelength/nm	Bandgap/eV
0.00	396	3.13
0.20	350	3.54
0.60	339	3.66
1.20	332	3.74

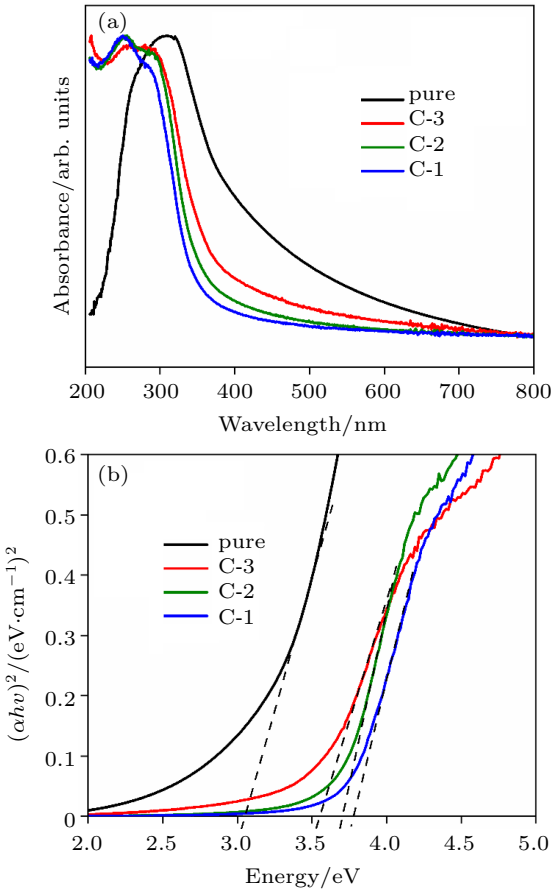


Fig. 6. (a) UV–vis absorption spectra, (b) Tauc plot of pure and carbon-doped TiO_2 NPs.

3.6. Electron paramagnetic resonance analysis

Electron paramagnetic resonance (EPR) is frequently considered to be a microwave absorption spectroscopy in which a microwave frequency radiation is absorbed by ions, molecules, or atoms having unpaired electrons. The EPR is the study of the interaction between electronic magnetic moments and the magnetic field at a fixed frequency. The splitting of energy levels into several lines within an atom in the presence of an external magnetic field is generally referred to as the Zeeman effect. Therefore, we may say that the EPR is the study of direct transitions between electronic Zeeman levels.[44]

The defect centers in pure and C-doped anatase TiO_2 NPs are investigated by using the X-band electron paramagnetic resonance spectrometer, equipped with a rectangular cavity TE_{102} (ADANI SPINSCAN X spectrometer). Figure 7 shows the EPR spectra of pure and C-doped TiO_2 samples taken at room temperature. The measurements are performed by varying the magnetic field in a range of 237–417 mT.

The g-factor for P (1.984), C-1 (1.987), C-2 (1.987), and C-3 (1.989) is calculated using the following equation:[45]

$$g = \frac{71.4477\nu}{B}, \tag{2}$$

where ν is the microwave frequency (in GHz) and B is the magnetic field (in mT) at the center of the signal. The EPR

signals with g-factor of 1.92–1.99 for pure and doped TiO_2 have been observed and are attributed to surface related Ti^{3+} centers associated with surface oxygen vacancies.[46] The effect of C doping in TiO_2 is also evident in the EPR spectra as shown in Fig. 7. It can be seen that the intensity of the resonance line decreases as the concentration of C increases. In C-doped TiO_2, EPR spectra broad signals at $g = 1.987$ and 1.989 are observed, which is a characteristic of trapped electrons in localized anatase Ti^{3+} surface states or Ti^{3+} associated with oxygen vacancies.[47]

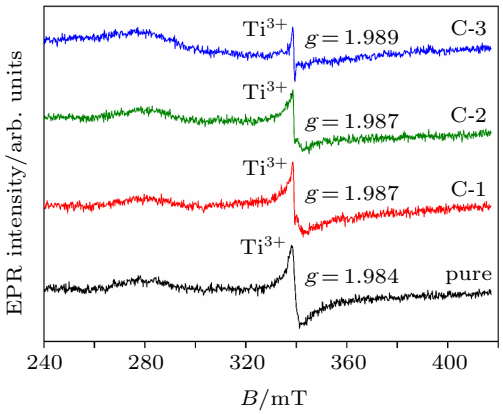


Fig. 7. Room temperature EPR spectra of pure and C-doped TiO_2 NPs.

Pure TiO_2 in ideal stoichiometry has Ti^{4+} ions, which are non-magnetic and ESR silent. However, the paramagnetic behavior in ESR spectra of the pure and C doped TiO_2 NPs indicates that paramagnetic response is resulted from the incorporation of defects, more likely oxygen vacancies, during the synthesis process. In oxide semiconductors, the origin of defect centers related to Ti^{3+} ions associated with oxygen vacancies (V_O) is still under debate due to its complex nature.[48] Such a center could be produced by different means, including reducing the samples in reducing atmospheres, illumination, and chemical doping, where vacancies are created during the process. During the illumination process, electrons are promoted to the valence band, thereby leading to Ti^{3+} ions, which are paramagnetic in nature. Among the defects generated by illumination, merely Ti interstitials and V_O can give excess electrons. Therefore, the observed resonance peaks are due to the formation of Ti^{3+}-V_O defect complexes.[48–50] Zhou *et al.* reported that the number of O vacancies is 1.5 times larger than that of Ti interstitials, and the formation of O vacancies is favored over the formation of Ti interstitials. Therefore, they concluded that each of the illuminations induces O vacancies, which leaves two electrons and changes the nearest Ti^{4+} ions to Ti^{3+} ions, resulting in Ti^{3+}-V_O defect complexes.[46] It is well known that O vacancies create charge imbalance and to compensate this induced charge around the defect, there is a chance to produce Ti^{2+} and/or Ti^{3+} ions of unpaired electrons (3d), which exhibits paramagnetic behavior or leads to the magnetic moment.[51,52]

4. Conclusion

In this work, a facile hydrothermal method has been employed to synthesize anatase TiO_2 spherical nanoparticles which evolve to elongated-shaped nanoparticles with the addition of carbon up to 1.2 mol% using glucose monohydrate ($C_6H_{12}O_6{\cdot}H_2O$). Via the XRD patterns, no structural changes were observed in nanostructured TiO_2 after doping with different concentrations of carbon, which confirms the formation of pure anatase phase of TiO_2 NPs. The crystallite sizes of pure and doped TiO_2NPs are calculated to be in the range of 13.3–14.7 nm. The UV–visible absorption spectra of the synthesized samples observed in the range of 200-800 nm illustrate a blueshift with increase in doping concentration. This clearly indicates the shift in bandgap towards higher values where the bandgap increases from 3.13 eV for pure TiO_2 to 3.74 eV with the increase in carbon concentration. The vibrational features and existence of fundamental functional groups in the as-prepared TiO_2 nanoparticles have been revealed by Raman spectroscopy and Fourier transform infrared spectroscopy, respectively. Furthermore, the X-band EPR spectra of pure and C-doped TiO_2 NPs indicate Ti^{3+} defect centers associated with oxygen vacancies (V_O).

References

[1] Khan A, Toufiq A M, Tariq F, Khan Y, Hussain R, Akhtar N and Rahman S U 2019 *Mater. Res. Express.* **6** 065043
[2] Wu Z, Yang S and Wu W 2016 *Nanoscale* **8** 1237
[3] Zhang G, Xiao X, Li B, Gu P, Xue H and Pang H 2017 *J. Mater. Chem. A* **5** 8155
[4] Pandey S C, Xu X, Williamson I, Nelson E B and Li L 2017 *Chem. Phys. Lett.* **669** 1
[5] Vardi N, Anouchi E, Yamin T, Middey S, Kareev M, Chakhalian J, Dubi Y and Sharoni A 2017 *Adv. Mater.* **29** 1605029
[6] Hong F, Yue B, Hirao N, Liu Z and Chen B 2017 *Sci. Rep.* **7** 44078
[7] Yin Z, Tordjman M, Lee Y, Vardi A, Kalish R and del Alamo J A 2018 *Sci. Adv.* **4** eaau0480
[8] Ye K, Li K, Lu Y, Guo Z, Ni N, Liu H, Huang Y, Ji H and Wang P 2019 *Trends Analyt Chem.* **116** 102
[9] Ye K, Li Y, Yang H, Li M, Huang Y, Zhang S and Ji H 2019 *Appl. Catal. B* **259** 118085
[10] Ye K H, Wang Z, Li H, Yuan Y, Huang Y and Mai W 2018 *Sci. China Mater.* **61** 887
[11] Huang Y, Guo Z, Liu H, Zhang S, Wang P, Lu J and Tong Y 2019 *Adv. Funct. Mater.* **29** 1903490
[12] Rahman M, Krishna K, Soga T, Jimbo T and Umeno M 1999 *J. Phys. Chem. Solids* **60** 201
[13] Beltran A, Gracia L and Andres J 2006 *J. Phys. Chem. B* **110** 23417
[14] Smith S J, Stevens R, Liu S, Li G, Navrotsky A, Boerio-Goates J and Woodfield B F 2009 *Am. Mineral.* **94** 236
[15] Zallen R and Moret M 2006 *Solid State Commun.* **137** 154
[16] Djarri A, Achour A, Soussou M A, Sobti N and Achour S 2018 *Mater. Charact.* **135** 139
[17] Barnard A and Curtiss L 2005 *Nano Lett.* **5** 1261
[18] Wu T, Kong W, Zhang Y, Xing Z, Zhao J, Wang T, Shi X, Luo Y and Sun X 2019 *small Methods* **3** 1900356
[19] Wu T, Zhu X, Xing Z, Mou S, Li C, Qiao Y, Liu Q, Luo Y, Shi X, Zhang Y and Sun X 2019 *Angew. Chem. Int. Ed.* **58** 18449
[20] Li B, Zhu X, Wang J, Xing R, Liu Q, Shi X, Luo Y, Liu S, Niu X and Sun X 2020 *Chem. Comm.* **56** 1074
[21] Hiroshi I, Yuka W and Kazuhito H 2003 *Chem. Lett.* **32** 772

[22] Wang J, Tafen D N, Lewis J P, Hong Z, Manivannan A, Zhi M, Li M and Wu N 2009 *J. Am. Chem. Soc.* **131** 12290

[23] Yan X, Yuan K, Lu N, Xu H, Zhang S, Takeuchi N, Kobayashi H and Li R 2017 *Appl. Catal. B* **218** 20

[24] Nyamukamba P, Tichagwa L and Greyling C 2012 *Mater. Sci. Forum* **712** 49

[25] Umebayashi T, Yamaki T, Itoh H and Asai K 2002 *Appl. Phys. Lett.* **81** 454

[26] Ren W, Ai Z, Jia F, Zhang L, Fan X and Zou Z 2007 *Appl. Catal. B* **69** 138

[27] Ali M, Hussain R, Tariq F, Noreen Z, Toufiq A M, Bokhari H, Akhtar N and ur Rahman S 2020 *Appl. Nanosci.* **10** 1005

[28] Shao J, Sheng W, Wang M, Li S, Chen J, Zhang Y and Cao S 2017 *Appl. Catal. B* **209** 311

[29] Noorimotlagh Z, Kazeminezhad I, Jaafarzadeh N, Ahmadi M, Ramezani Z and Martinez S S 2018 *J. Hazard. Mater.* **350** 108

[30] Al-Degs Y S, El-Barghouthi M I, El-Sheikh A H and Walker G M 2008 *Dyes Pigm.* **77** 16

[31] Yang G, Jiang Z, Shi H, Xiao T and Yan Z 2010 *J. Mater. Chem.* **20** 5301

[32] Abdullah A M, Al-Thani N J, Tawbi K and Al-Kandari H 2016 *Arab. J. Chem.* **9** 229

[33] Sim L C, Leong K H, Ibrahim S and Saravanan P 2014 *J. Mater. Chem. A* **2** 5315

[34] Attar A S, Ghamsari M S, Hajiesmaeilbaigi F and Mirdamadi S 2008 *J. Mater. Sci.* **43** 1723

[35] Toufiq A M, Wang F, Li Q and Li Y 2014 *Appl. Phys. A* **116** 1127

[36] Shaban M, Ashraf A M and Abukhadra M R 2018 *Sci. Rep.* **8** 781

[37] Ratova M, Klaysri R, Praserthdam P and Kelly P J 2018 *Vacuum* **149** 214

[38] Lin H, Huang C, Li W, Ni C, Shah S I and Tseng Y H 2006 *Appl. Catal. B* **68** 1

[39] Brus L E 1984 *J. Chem. Phys.* **80** 4403

[40] Rino J-P and Studart N 1999 *Phys. Rev. B* **59** 6643

[41] Bhange P, Awate S, Gholap R, Gokavi G and Bhange D 2016 *Mater. Res. Bull.* **76** 264

[42] Linsebigler A L, Lu G and Yates Jr J T 1995 *Chem. Rev.* **95** 735

[43] Lu X H, Huang X, Xie S L, Zheng D Z, Liu Z Q, Liang C L and Tong Y X 2010 *Langmuir* **26** 7569

[44] Pham C V, Krueger M, Eck M, Weber S and Erdem E 2014 *Appl. Phys. Lett.* **104** 132102

[45] Lund A, Shiotani M and Shimada S 2011 *Principles and applications of ESR spectroscopy* (New York: Springer) p. 91

[46] Zhou S, Čižmár E, Potzger K, Krause M, Talut G, Helm M, Fassbender J, Zvyagin S, Wosnitza J and Schmidt H 2009 *Phys. Rev. B* **79** 113201

[47] Hurum D C, Gray K A, Rajh T and Thurnauer M C 2005 *J. Phys. Chem. B* **109** 977

[48] Ogale S B 2010 *Adv. Mater.* **22** 3125

[49] Tian Y, Bakaul S R and Wu T 2012 *Nanoscale* **4** 1529

[50] Peng H, Li J, Li S S and Xia J B 2009 *Phys. Rev. B* **79** 092411

[51] Yoon S D, Chen Y, Yang A, Goodrich T L, Zuo X, Arena D A, Ziemer K, Vittoria C and Harris V G 2006 *J. Phys.: Condens. Matter* **18** L355

[52] Hong N H, Sakai J, Poirot N and Brizé V 2006 *Phys. Rev. B* **73** 132404